


Article

Correlation between Temperature and the Posture of Transmission Line Towers

Minzhen Wang¹, Haihang Gao², Zhigang Wang³, Keyu Yue³, Caiming Zhong¹, Guangxin Zhang¹ and Jian Wang^{4,5,6,*} 

- ¹ College of Science and Technology, Ningbo University, Ningbo 315300, China; wangminzhen@nbu.edu.cn (M.W.); zhongcaiming@nbu.edu.cn (C.Z.); zhangguangxin@nbu.edu.cn (G.Z.)
- ² School of Electrical and Information Engineering, Changchun Institute of Technology, Changchun 130012, China; gaohaihang@stu.ccit.edu.cn
- ³ State Grid Jilin Province Electric Power Co., Ltd., Liaoyuan Power Supply Company, Liaoyuan 136200, China; wangzhg02@jl.sgcc.com.cn (Z.W.); lyyueky@jl.sgcc.com.cn (K.Y.)
- ⁴ School of Mathematics and Statistics, Nanjing University of Information Science and Technology, Nanjing 210044, China
- ⁵ Center for Applied Mathematics of Jiangsu Province, Nanjing University of Information Science and Technology, Nanjing 210044, China
- ⁶ Jiangsu International Joint Laboratory on System Modeling and Data Analysis, Nanjing University of Information Science and Technology, Nanjing 210044, China
- * Correspondence: 003328@nuist.edu.cn

Abstract: Ensuring the safety of transmission line towers is vital for human safety, power supply, economic development, and environmental protection. This study specifically examines how temperature affects tower inclination. Multifractal detrended cross-correlation analysis (MF-DCCA) is a combination of multifractal detrended fluctuation analysis (MF-DFA) and DCCA that reveals the multifractal features of two cross-correlated non-stationary signals. This paper adopts the MF-DCCA tool to investigate the cross-correlations between the internal temperature of an inclination sensor device and the posture of a transmission line tower. The tilt angle data in the x- and y-axes are used to measure the posture of the transmission line tower. We start by using Pearson correlation to assess the relationship between temperature and two inclination angles, followed by verifying their correlation with a p -value below 0.05 using first-order linear fitting. We initially assess the multifractal features of three time series using MF-DFA before MF-DCCA analysis. All exhibit multifractal traits with $H(2) < 0.5$, indicating negative persistence, especially notable in the temperature series. Finally, we adopt the MF-DCCA approach to examine the multifractal cross-correlation between tilt-angle time series and temperature time series, and the results indicate the negative persistence of the cross-correlation between the time series. Furthermore, the multifractal cross-correlation of temperature and inclination data on the y-axis was also found to be stronger than on the x-axis based on features of the scaling exponent and symmetry exponent.

Keywords: transmission line tower; temperature; tilt angle; cross-correlation



Citation: Wang, M.; Gao, H.; Wang, Z.; Yue, K.; Zhong, C.; Zhang, G.; Wang, J. Correlation between Temperature and the Posture of Transmission Line Towers. *Symmetry* **2024**, *16*, 1270. <https://doi.org/10.3390/sym16101270>

Academic Editor: Constantin Fetecau

Received: 23 August 2024

Revised: 24 September 2024

Accepted: 25 September 2024

Published: 26 September 2024



Copyright: © 2024 by the authors. Licensee MDPI, Basel, Switzerland. This article is an open access article distributed under the terms and conditions of the Creative Commons Attribution (CC BY) license (<https://creativecommons.org/licenses/by/4.0/>).

1. Introduction

Transmission line towers are pole- or tower-shaped structures that support overhead transmission line conductors, and overhead ground wires, maintaining a certain distance between these and the earth. As a pillar industry of national economies, the power industry and power grid construction have spread to every country, so the requirements for the safe and stable operation of transmission line towers are gradually increasing. Steel structures, wooden structures, and reinforced concrete structures are used for transmission towers in various countries around the world. The rated power of wooden structure transmission towers depends on the load-bearing capacity of the materials and the design of the structure. They are typically used for shorter-distance transmission lines or in

areas where environmental conservation factors need to be considered. For example, the “Varrebergsmasten” in Sweden. Usually, wooden and reinforced concrete pole-shaped structures are called simply poles, while tower-shaped steel structures and reinforced concrete chimney-shaped structures are called towers. However, which specific design to adopt depends on available natural resources, climate conditions, and the geographical location of each country. For example, low temperatures can easily affect the stability of steel structures, leading to damage to tower structures. Therefore, it is of great significance to study the attitude status of iron towers in the northern cold regions, which also requires real-time monitoring of the internal temperature of inclination sensor devices and tilt angle of transmission towers, and analysis of their dynamic characteristics and correlation.

Due to the importance of transmission line towers for the development of modern society, recently, many scholars have conducted extensive research on transmission line towers [1–5]. Wang et al. [6] studied the seasonal variation in tower base impedance by measuring the annual tower base impedance of several types of transmission line grounding systems in Canadian hydropower stations. In order to ensure the safety of live working personnel and reduce the consumption of test resources, Gao et al. [7] studied air-gap discharge during the GPLW process of transmission lines. Many researchers have also paid attention to the relationship between transmission towers and temperature. The process of and trend in ground temperature changes around the foundation of a Qinghai Tibet transmission line tower were studied in [8]. This study revealed the process of and trend in ground temperature changes, which plays a significant role in evaluating the evolution of thermal conditions around tower foundations under the background of climate change. Rezaei et al. [9] also analyzed the impact of climate change on the reliability of overhead transmission lines. They found that historical climate data may not be sufficient to ensure the reliability of future transmission line systems, and the design of existing or new lines should be evaluated by combining climate models and historical climate data.

Refs. [6,9] both considered the impact of climatic factors on power transmission systems, but their approaches differ from the focus of this study. Ref. [6] primarily assesses the effect of climate-related disasters on the operational efficiency of transmission towers without further investigating the gradual changes in tower structures under normal low-temperature conditions. The article addresses damage to certain structural components in extreme cold scenarios that result in transmission failures but does not provide a detailed explanation for the inclination of transmission towers caused by climatic factors. Ref. [9] examines the influence of seasonal climate on transmission systems, but the study focuses on how seasonal factors affect grounding systems rather than the transmission towers themselves.

Thus, there is currently a research gap regarding the influence of temperature and tower shape on transmission towers, notably a lack of statistical analysis on tower tilt angle and real-time temperature data in the region. This study focuses on analyzing temperature dynamics and tower posture data using multifractal detrended cross-correlation analysis (MF-DCCA) [10]. MF-DCCA, a combination of multifractal detrended fluctuation analysis [11] and detrended cross-correlation analysis [12], is commonly used to explore the impact of various factors on the relationships between multiple temporal variables in a system. Multifractal models, known for revealing hidden multifractal characteristics in non-stationary time series, have found wide applications in diverse fields such as finance [13–15], biomedicine [16–18], nature language processing [19], transportation [20], and meteorology [21,22]. In [23], the authors employed a non-linear cross-correlation method to study the relationship between water level and water temperature. Additionally, they used the MF-DCCA method to prove that there is a multifractal cross-correlation between the time series of water level and water temperature. Considering the nonlinearity and complexity of electricity consumption and pollutant emission data of industrial enterprises, Li et al. [24] used MF-DCCA to show that there is indeed a correlation between electricity consumption data and pollutant emission levels of enterprises.

The structure of the rest of this article is as follows. In Section 2, we provide a comprehensive overview of three analytical methods: Pearson correlation analysis, MF-DFA, and MF-DCCA. In Section 3, we describe the process of data collection. In Section 4, we determine the correlation between tilt angle and the internal temperature of an inclination sensor device. Finally, conclusions are drawn in Section 5.

2. Methodology

2.1. Pearson Correlation Analysis

Pearson correlation analysis is a statistical method used to measure the linear relationship between two continuous variables. Its primary purpose is to assess the strength and direction of correlation between two variables, whether and how they are linearly related. Pearson correlation analysis is roughly divided into the following steps:

Step 1: The two sets of sample data are designated as X_i and Y_i , $i = 1, 2, \dots, n$. Continuing with the examination of whether the two variables adhere to a normal distribution, various methods such as the Jarque–Bera Test, Shapiro–Wilk test, Kolmogorov–Smirnov test, etc., can be employed.

Step 2: The formula for calculating the Pearson correlation coefficient r is as follows:

$$r = \frac{\sum_{i=1}^n (X_i - \bar{X})(Y_i - \bar{Y})}{\sqrt{\sum_{i=1}^n (X_i - \bar{X})^2} \sqrt{\sum_{i=1}^n (Y_i - \bar{Y})^2}}, \quad (1)$$

where \bar{X} represent the average of X_i and \bar{Y} represent the average of Y_i . The variable r takes values in the range of -1 to 1 , where 1 indicates perfect positive correlation, -1 indicates perfect negative correlation, and 0 indicates no linear relationship.

Step 3: Defining the degrees of freedom as $\eta = n - 2$. To assess significance, calculate the p -value for the correlation test. Firstly, calculate the t -statistic as

$$T = r \sqrt{\frac{\eta}{1 - r^2}}. \quad (2)$$

Subsequently, utilize the “tcdf” function in MATLAB software to compute the cumulative distribution of the sample \hat{t} , and substitute the result into the formula to derive the p -value,

$$p = 2(1 - \hat{t}). \quad (3)$$

Assuming a significance level of 0.05 , if the calculated p -value is less than the significance level, the correlation is considered significant. If the p -value is greater than the significance level, the correlation is deemed non-significant.

2.2. MF-DFA

MF-DFA is an advanced method designed for analyzing the multifractal properties of signals and time series. It extends the capabilities of DFA. The primary objective of MF-DFA is to conduct a comprehensive analysis of the multifractal features inherent in signals. This method proves invaluable in unveiling the complex and multiscale structures present in signals across various time scales and is one of the important methods for multifractal characteristics, which has been widely applied in various fields [25–27].

The algorithm steps of MF-DFA can be roughly divided into five stages, summarized as follows: constructing time series, dividing non-overlapping windows, fitting the series, obtaining q -th-order fluctuation function, and calculating the fractal degree.

Step 1: Given a time series $t(i)$ for $i = 1, 2, \dots, N$ where N is the total length of the series, and let \bar{t} represent the average of t . Then, we can construct a new series as

$$P(i) = \sum_{k=1}^i \{t(k) - \bar{t}\}, \quad i = 1, 2, \dots, N. \quad (4)$$

Step 2: Divide the profile $P(i)$ into $A_s \equiv \text{int}(\frac{N}{s})$ non-overlapping windows of equal length s . To ensure the processing of all data, perform the same procedure starting from the end of the sequence, resulting in a total of $2A_s$ windows.

Step 3: Perform least-squares fitting for each window by utilizing $y_v^m(i)$ to represent the m -th order polynomial for the v -th window. Subsequently, compute the residuals between the original sequence $P(i)$ and the fitted polynomial $y_v^m(i)$. This process yields the fluctuation function for each window, as given by the equation

$$F^2(s, v) = \frac{1}{s} \sum_{i=1}^s \{P[N - (v - N_s)s + i] - y_v^m(i)\}^2, \quad (5)$$

where $v, v = A_s + 1, A_s + 2, \dots, 2A_s$.

Averaging over the $2A_s$ windows gives the q -th-order fluctuation function. The fractal order q can take any real value, when $q = 2$, MF-DFA degenerates to DFA.

$$F_q(s) = \begin{cases} \left\{ \frac{1}{2A_s} \sum_{v=1}^{2A_s} [F^2(s, v)]^{\frac{q}{2}} \right\}^{\frac{1}{q}}, & \text{if } q \neq 0, \\ \exp\left\{ \frac{1}{4N_s} \sum_{v=1}^{2A_s} \ln[F^2(s, v)] \right\}, & \text{if } q = 0. \end{cases} \quad (6)$$

Step 4: Iterating through steps 2 to 3. It becomes evident that the magnitude of $F_q(s)$ increases as s increases. Different values of q characterize the impact of various levels of fluctuations on $F_q(s)$. For $q < 0$, the magnitude of $F_q(s)$ is primarily influenced by the small fluctuation deviation $F^2(s, v)$, whereas for $q > 0$, it is mainly influenced by the large fluctuation deviation $F^2(s, v)$.

Step 5: As s increases, F_q follows a power-law relationship, denoted by $F_q(s) \propto s^{H(q)}$. When $q = 2$, we label F_q as the standard DFA, with $H(q)$ representing the generalized Hurst exponent. The diversity of the original sequence hinges on the value of $H(q)$. If $H(q)$ remains constant across different q values, the sequence is a single fractal. Conversely, if $H(q)$ varies with q , it demonstrates multifractal features, also referred to by the generalized Hurst exponents. When $H(q) = 0.5$, this indicates that the time series exhibits characteristics of a random walk, implying the absence of persistent trends or long-term correlations. For $H(q) > 0.5$, this signifies positive persistence in the time series, suggesting a more pronounced trend. Conversely, for $H(q) < 0.5$, this denotes negative persistence, implying a higher likelihood of trend reversals in the time series. Subsequently, the degree of multifractality can be quantified as

$$\Delta H = H_{\max}(q) - H_{\min}(q). \quad (7)$$

Moreover, the multifractality can also be described by the scaling exponent $\tau(q)$. The scaling exponent $\tau(q)$ is related to the generalized Hurst exponent $h(q)$ and the topological dimension D_u of the multifractal series; the scaling exponent is defined as

$$\tau(q) = qH(q) - D_u, \quad (8)$$

and for a one-dimensional time series, that is $D_u = 1$, the scaling exponent is changed to

$$\tau(q) = qH(q) - 1. \quad (9)$$

The parameter α represents the singularity strength and $f(\alpha)$ denotes the fractal dimension of the subset of the time series with singularities of strength equal to α . The $f(\alpha)$ spectrum is connected to $h(q)$ through the Legendre transformation,

$$\alpha = \tau'(q) = H(q) + H'(q), \quad (10)$$

$$f(\alpha) = q\alpha - \tau(q) = q[\alpha - H(q)] + 1. \quad (11)$$

The determination of whether a studied sequence possesses multifractal properties, as characterized by α and $f(\alpha)$, generally follows the following rules: for a monofractal sequence, $f(\alpha)$ is constant, while for a multifractal sequence, $f(\alpha)$ exhibits a unimodal bell pattern. The degree of multifractality can be quantified by

$$\Delta\alpha = \alpha_{\max} - \alpha_{\min}. \quad (12)$$

In general, a larger maximum value of $f(\alpha)$ corresponds to a larger $\Delta\alpha$, indicating a stronger degree of multifractality in the studied sequence.

2.3. MF-DCCA

MF-DCCA is employed to analyze the multiscale interrelationship between two time series, particularly in the financial domain. Similar to MF-DFA, the MF-DCCA method can be carried out in the following five steps.

Step 1. Consider two time series x_j and y_j , for $j = 1, 2, \dots, M$. The cumulative sequence of the original time series is constructed as follows

$$Q(j) = \sum_{m=1}^j (x_m - \frac{1}{M} \sum_{t=1}^M x_t), j = 1, 2, \dots, M, \quad (13)$$

$$G(j) = \sum_{m=1}^j (y_m - \frac{1}{M} \sum_{t=1}^M y_t), j = 1, 2, \dots, M. \quad (14)$$

Step 2. Divide the new sequences $Q(j)$ and $G(j)$ into non-overlapping segments of equal scale s , resulting in a total of $M_s = \text{int}(\frac{M}{s})$ segments. To ensure comprehensive information retention, the division process is applied symmetrically from both ends of the sample. Following two identical segmentation operations, each series ultimately yields $2B_s$ segments.

Step 3. Each subsegment is fitted by the least-squares method, and the k -th-order fitting polynomial of each subsegment is obtained as follows

$$Q_v^{\wedge}(i) = a_1 i^k + a_2 i^{k-1} + \dots + a_k i + a_{i+1}, i = 1, 2, \dots, s, \quad (15)$$

$$G_v^{\wedge}(i) = b_1 i^k + b_2 i^{k-1} + \dots + b_k i + b_{i+1}, i = 1, 2, \dots, s. \quad (16)$$

Step 4. Calculate the covariance sequence after local trend separation.

$$\Phi^2(s, v) = \frac{1}{s} \sum_{i=1}^s \left\{ |Q[(v-1)s+i] - Q_v^{\wedge}(i)| |G[(v-1)s+i] - G_v^{\wedge}(i)| \right\}, \quad (17)$$

for each subsegment, $v, v = 1, 2, \dots, M_s$ and

$$\Phi^2(s, v) = \frac{1}{s} \sum_{i=1}^s \left\{ |Q[M - (v - M_s)s + i] - Q_v^{\wedge}(i)| \cdot |G[M - (v - M_s)s + i] - G_v^{\wedge}(i)| \right\}, \quad (18)$$

for $v = M_s + 1, M_s + 2, \dots, 2M_s$.

Step 5. Calculate the q -th-order fractal detrended wave function $F_q(s)$ on the whole time series, as follows

$$F_q(s) = \begin{cases} \left\{ \frac{1}{2M_s} \sum_{v=1}^{2M_s} [\Phi^2(s, v)]^{\frac{q}{2}} \right\}^{\frac{1}{q}}, & \text{if } q \neq 0, \\ \exp \left\{ \frac{1}{2M_s} \sum_{v=1}^{2M_s} \ln[\Phi^2(s, v)] \right\}, & \text{if } q = 0. \end{cases} \quad (19)$$

We can obtain the relationship between the wave function $F_q(s)$ and Hurst exponent $H_{xy}(q)$ calculated by MF-DCCA through $F_q(s) \propto s^{H_{xy}(q)}$, where q and g represent two time series. For $q = 2$, it is the familiar Hurst exponent. $H_{xy}(q) > 0.5$ indicates persistent cross-correlation: if $\{x_j\}$ rises, $\{y_j\}$ is likely to rise. $H_{xy}(q)$ signals anti-persistent cross-correlation: if $\{x_j\}$ rises, $\{y_j\}$ likely falls. If $H_{xy}(q) = 0.5$, no correlation exists. Variable q represents fluctuation size; multifractality occurs if $H_{xy}(q)$ varies with q , otherwise, it is monofractal.

In addition, $\tau_{xy}(q)$ is another method to characterize the multifractal scaling behavior. The relationship between $H_{xy}(q)$ and mass exponent $\tau_{xy}(q)$ can be obtained through MF-DFA as follows

$$\tau_{xy}(q) = qH_{xy}(q) - 1. \quad (20)$$

The singularity spectrum $f_{xy}(\alpha)$ of the Holder exponent α_{xy} is another widely used indicator for measuring the multifractality of any two time series and can be defined as

$$\alpha = H_{xy}(q) + qH'_{xy}(q), \quad f_{xy}(\alpha) = q[\alpha_{xy} - H_{xy}(q)] + 1. \quad (21)$$

Similar to MF-DFA, where α_{xy} represents the singularity strength, we define

$$\Delta\alpha_{xy} = \alpha_{xy_{max}} - \alpha_{xy_{min}}, \quad (22)$$

which is an indicator of multifractal degree. According to [28], the larger $\Delta\alpha_{xy}$, the stronger the multifractal degree, indicating a more uneven data distribution. $f_{xy}(\alpha)$ is the multifractal spectrum representing the aggregation with the same singularity strength α_{xy} . The multifractal spectrum of a type of data or system may exhibit symmetry if the type of data or system has desirable self-similarity and this property is uniformly distributed on all scales. In investigating the multifractal spectrum, researchers would take into account the symmetry of the objective or system because symmetry can provide important information about the internal structure and nature of the system to better understand the object or system under research. The multifractal spectrum exhibits a certain symmetry which depends on $\alpha_{xy_{max}}$, $\alpha_{xy_{min}}$ and α_0 , where α_0 corresponds to the maximum of $f_{xy}(\alpha)$. If $\alpha_{xy_{max}} - \alpha_0 = \alpha_0 - \alpha_{xy_{min}}$, then the spectrum is symmetric, if $\alpha_{xy_{max}} - \alpha_0 > \alpha_0 - \alpha_{xy_{min}}$, then the spectrum is right skewed, and if $\alpha_{xy_{max}} - \alpha_0 < \alpha_0 - \alpha_{xy_{min}}$, then the spectrum is left skewed. The symmetry exponent could be shown as: $(\alpha_{xy_{max}} - \alpha_0 - (\alpha_0 - \alpha_{xy_{min}})) / \Delta\alpha_{xy}$. A larger symmetry exponent indicates greater variation in mean density variation over the region and greater multiple fractality of the sequence.

All the calculations are performed using MATLAB R2020a on an Intel(R) Core(TM) i5-6200 CPU 2.30 GHz processor.

3. Data Collection

Tower tilting poses a great threat to the power grid. In order to effectively prevent tower tilting accidents, it is necessary to monitor the condition of the tower in real time. By collecting data such as the longitudinal tilt angle, transverse tilt angle, and comprehensive tilt angle of the tower, wireless transmission can be sent to the monitoring center, which can help workers detect abnormal situations in a timely manner. We use a high-precision dual axis tilt sensor ZCT330Mx SWP-N-YK based on the NB-IoT wireless network for data collection. A schematic diagram of the vertical and horizontal inclination angles of the tower is shown in Figure 1.

The sensor has a resolution of 0.001° , ensuring it is able to capture subtle angular changes. Under ambient temperatures ranging from -15°C to $+15^\circ\text{C}$, the sensor's accuracy is $\pm 0.005^\circ$, while within the temperature range -30°C to $+30^\circ\text{C}$, the accuracy is $\pm 0.01^\circ$. Temperature variations have minimal impact on the sensor's zero point, with a typical zero-point drift of $\pm 0.002^\circ / ^\circ\text{C}$ and a maximum drift of $\pm 0.2^\circ / ^\circ\text{C}$. The sensor is

capable of operating over a wide temperature range from $-40\text{ }^{\circ}\text{C}$ to $+85\text{ }^{\circ}\text{C}$, making it suitable for use in various harsh environmental conditions.

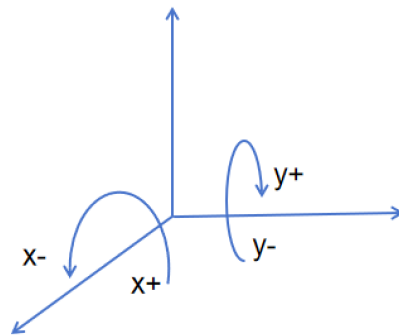
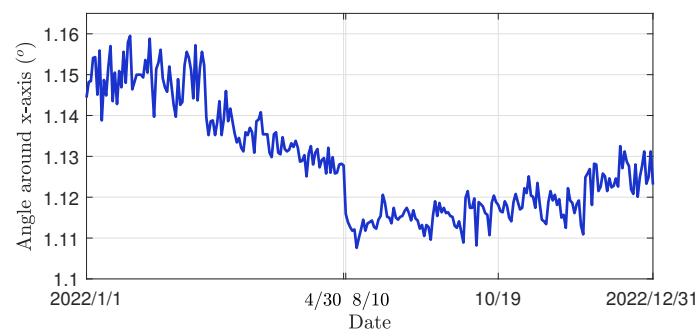
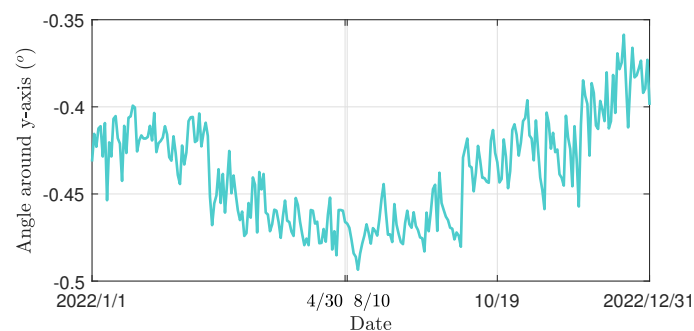


Figure 1. Schematic diagram of the inclination angle between the transmission tower and the x/y-axis.

The collected data also include internal temperature data of the inclination sensor device. The internal temperature of the inclination sensor device reflects the air temperature in the monitoring area. The data collection area is located in Jilin Province, China. The period covers from 1 January 2022 to 31 December 2022. Due to our main investigation being into the influence of low temperature on the inclination of transmission towers, we removed data from the high temperature period between 1 May 2022 and 9 August 2022, and used 261 pieces of data for analysis. The time series of the tilt angle with respect to the x- and y-axes and the time series of temperature are shown in Figure 2. It can be seen from the collected data that the three sets of data have a certain symmetry, and all reach the maximum value near the central axis. We use the skewness function to calculate the skewness of the data. When the absolute value of skewness is less than 0.5, we consider the data to be approximately symmetric. Upon testing, the skewness of all three datasets was found to be less than 0.2, which can be used as evidence to demonstrate that the data are roughly symmetric.



(a)



(b)

Figure 2. Cont.

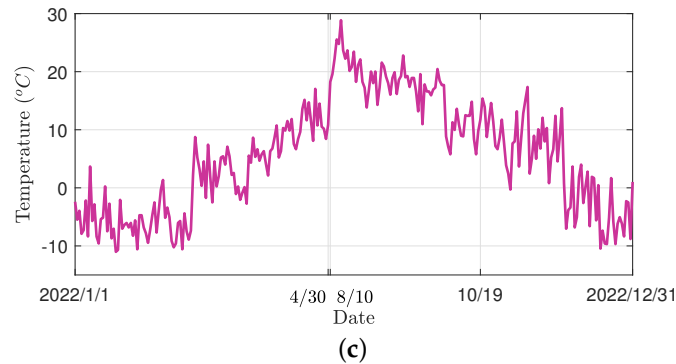


Figure 2. The original time series of (a) x-axis inclination angle, (b) y-axis inclination angle, and (c) temperature time series.

From Figure 2, it can be seen that the trend in the time series of the x-axis inclination angles and the temperature time series show opposite trends. It is worth mentioning that since the y-axis inclination angle is negative, a large negative number indicates a larger angle. Thus, the trend in the time series of y-axis tilt angle is consistent with the temperature time series. Low temperatures can result in soil freezing and expansion, leading to foundation movement or uneven settling, which can cause tower tilting. Additionally, thermal contraction occurs in the materials of transmission towers. This thermal contraction of materials can induce uneven stress distribution in certain parts of the structure, contributing to tower tilting [29].

4. Empirical Analysis

In this section, we preliminarily determine the correlation between tilt angle and the internal temperature of the inclination sensor device. We utilize the Pearson correlation coefficient to check the correlations, as shown in Table 1. We only count the average daily temperatures in an area, and the combined temperatures over the course of a year fit a normal distribution [30]. As the tower data only covers the low-temperature portion, normality testing is not conducted here. However, similar to the temperature data, the tower data exhibits symmetric distribution and is highly correlated with the temperature sequence. Therefore, if the tower dataset were to encompass data for the entire year, it should also demonstrate a normal distribution. In addition, we tested the linearity of the two sets of time series to qualify for the use of Pearson correlation analysis. In Figure 3, we show scatter plots of inclination angle and temperature in two directions. The results show a strong correlations between tilt angles and temperature, and a negative correlation between x-axis tilt angle and temperature, meaning that the higher the temperature, the smaller the x-axis tilt angle. In addition, for the y-axis tilt angle, the absolute value of the angle should be considered, so here the y-axis tilt angle is positively correlated with temperature, that is, the lower the temperature, the smaller the y-axis tilt angle. From Table 1, it can be observed that the absolute values of the Pearson correlation coefficients between temperature and the x-axis and y-axis rotation angles are both greater than 0.7. This indicates a strong linear relationship between the two variables. Consequently, with changes in temperature, it is highly probable that the tower tilt angles will also vary. In addition, we present a linear fitting relationship based on the data, as shown by the blue dashed line in Figure 3. We also conduct a p -value test on the linear regression model: if $p < \alpha$ (α determines the level of significance), this indicates a significant linear correlation between the dependent variable and the independent variable. The results show that p is much smaller than 0.05.

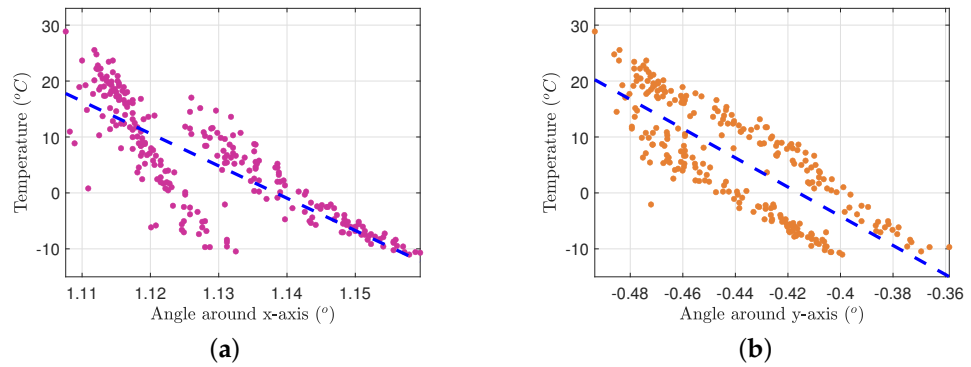


Figure 3. The first-order linear fitting between the temperature data and (a) x-axis tilt angle data, and (b) y-axis tilt angle data. A color version of the figure is available in the web version of the article.

Table 1. Pearson correlation between temperature and tilt angle data.

Series Pair	Pearson Correlation	p-Value
Temperature/Angle around x-axis (°)	−0.8054	8.99×10^{-61}
Temperature/Angle around y-axis (°)	−0.7934	9.04×10^{-58}

Subsequently, before exploring the cross-correlations between tilt angles and temperature, we first adopt cross-correlation test statistic $Q_{cc}(m)$ [31] to prove the existence of correlation between sequences. The specific definition of $Q_{cc}(m)$ is as follows.

$$Q_{cc}(m) \equiv n^2 \sum_{i=1}^m \frac{P_i^2}{n-i}, P_i = \frac{\sum_{k=i+1}^n x_k y_{k-i}}{\sqrt{\sum_{k=1}^n x_k^2 \sum_{k=1}^n y_k^2}} \tag{23}$$

where m is the degree of freedom, and n is the length of the time series x and y . $Q_{cc}(m)$ is approximately $\chi^2(m)$ distributed with degree of freedom m . Here, we set critical value for $\chi^2(m)$ distribution at a 5% level of significance. In Figure 4, we observe that $Q_{cc}(m)$ of both time-series pairs exceed the critical value, indicating significant cross-correlations between the tilt angles and temperature time series.

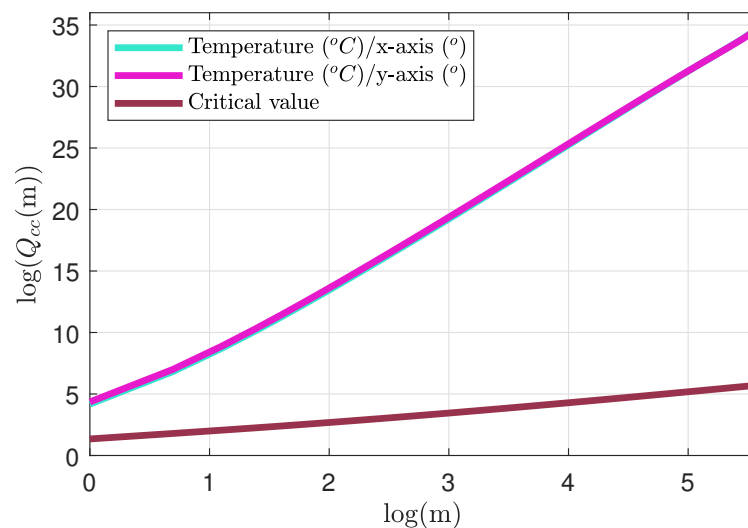


Figure 4. Cross-correlation statistics $\log(Q_{cc}(m))$ of two time-series pairs. A color version of the figure is available in the web version of the article.

Next, before conducting MF-DCCA, we perform multifractal detrend fluctuation analysis on the three sequences to check for the presence of multifractal characteristics, respectively. Based on the characteristics of the three sequences in Figure 2, we use the logarithmic sequence (i.e., $\log(x_{i+1}) - \log(x_i)$) as the original sequences. In addition, to avoid computational errors, we first regularize the values of the original data in the interval $[1.001, 2.001]$, which does not change the trend of the sequences or the correlation between sequences. The first-order detrending polynomial is selected to carry out the analysis of the MF-DFA, $q = -10, -9, \dots, 9, 10$. In addition, the time scale s varies from 5 to 15. The fluctuation functions plots between $\log(s)$ and $\log(F_q(s))$ are shown in Figure 5. We see that the fluctuation values increase as the segments increase, and the slope decreases as q increases, showing that multifractal properties exist in all the three time series. In addition, compared to large segment sizes, fluctuations are more pronounced at small segment sizes.

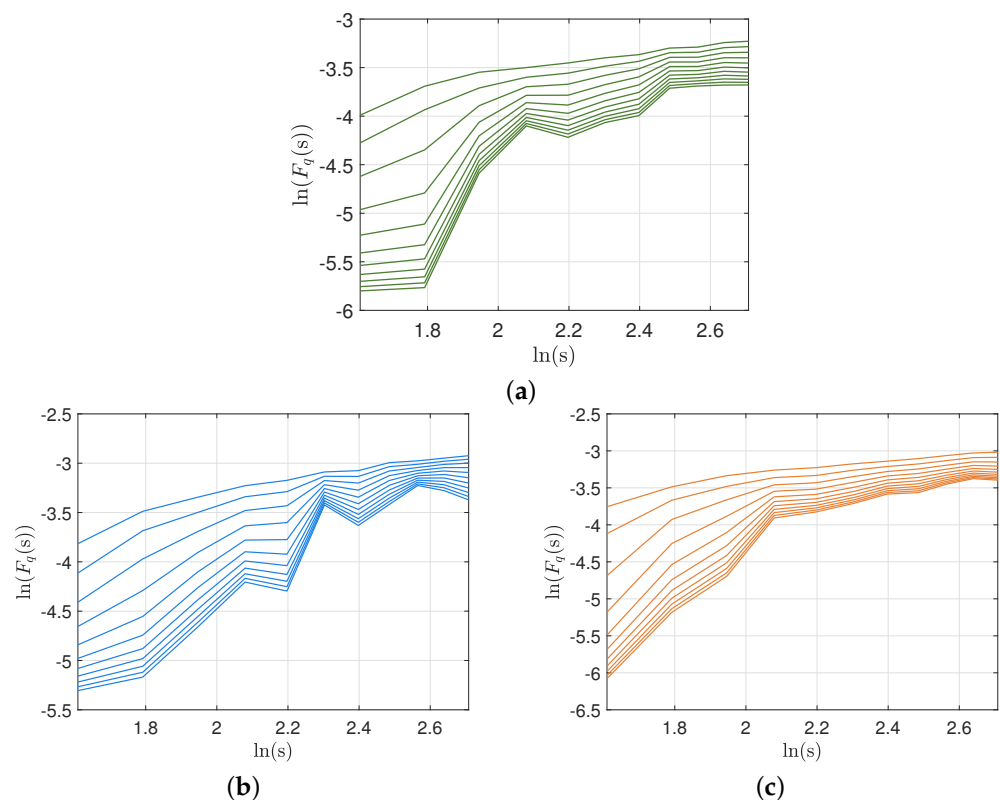


Figure 5. Double logarithmic curves between the fluctuation value and segment size of (a) x-axis inclination angle, (b) y-axis inclination angle, and (c) temperature time series.

Based on the slope of the curve in Figure 5, we obtain the generalized Hurst exponent of three sequences in Figure 6a. The decreasing $H(q)$ indicates that the three time series are not monofractal. We notice that when $q < 0$, the values of $H(q)$ are all greater than 0.5, indicating that all three time series have positive persistence in small fluctuations. However, when $q > 0$, most of the $H(q)$ values are less than 0.5, implying that the trend in the time series will change when there is a large fluctuation. Persistent negative trends suggest that the inclination of the tower exhibits alternating variations over different periods. This indicates that the tower's tilt is significantly influenced by external environmental factors, which themselves are subject to fluctuations [32,33]. These fluctuations are therefore reflected in the variations in the tilt angle. This discovery is also consistent with reality, showing that the tilt angle will change in the opposite direction to the original trend with large temperature fluctuations, and the trend in the temperature time series will change with seasonal fluctuations. In addition, the difference between the maximum H and the minimum H can also reflect the stability of the time series. The larger the ΔH , the more unstable the time series. Here, we can see that the stability of the two tilt-angle time series

are similar, and both are more stable than the temperature time series. This conclusion can also be obtained from the curvature of the τ_q curve and the width of $f(\alpha)$, as shown in Figure 6b,c. Additionally, it is shown in Figure 6c that the multifractal spectrum sharply skews towards the right with asymmetry. A right-skewed spectrum indicates that there are many areas of gradual change within the signal or dataset, with fewer regions of abrupt change. This reflects that in the measured region, most weather variations occur gradually and continuously, while extreme weather events are relatively rare. In the context of tower-tilt variations, this suggests that we can focus more on stable trends rather than sudden events, thereby improving long-term trend forecasting capabilities.

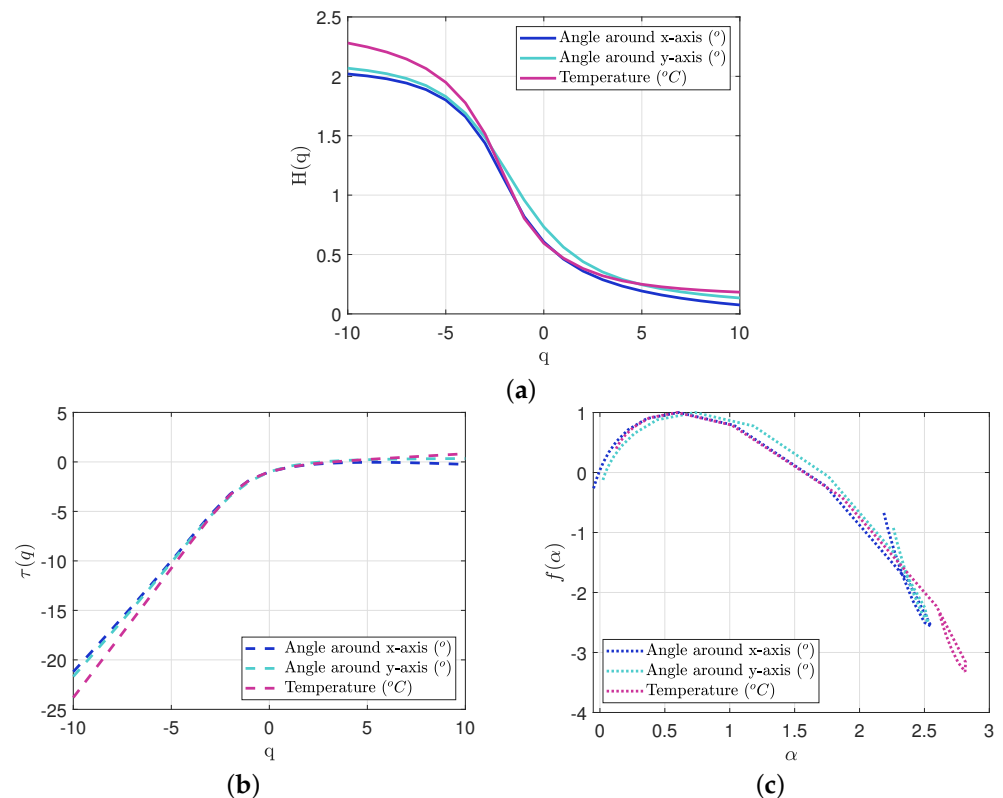


Figure 6. (a) The generalized Hurst exponent, (b) Renyi exponent, and (c) multifractal spectrum of three time series by MF-DFA.

Next, we use MF-DCCA to explore the cross-correlation characteristics between the tilt-angle time series and temperature time series. We depict the generalized Hurst exponent, Renyi exponent, and multifractal spectrum between the tilt angle time series and temperature time series in Figure 7. Figure 7a shows that both $H_{xy}(2)$ values are less than 0.5, suggesting that both the time series of x-axis tilt angle and y-axis tilt angle have a negative persistence of cross-correlations with temperature time series. We also observe that the ΔH_{xy} of “Temperature (°C)/y-axis (°)” is larger than that of the time-series pair “Temperature (°C)/x-axis (°)”, which implies a greater cross-correlations of multifractality between temperature and y-axis tilt angle time series. Figure 7b,c can also support this point. The curves in Figure 7c is asymmetrically upconvex and skewed towards the right, which shows that the sequence possesses multiple fractal features.

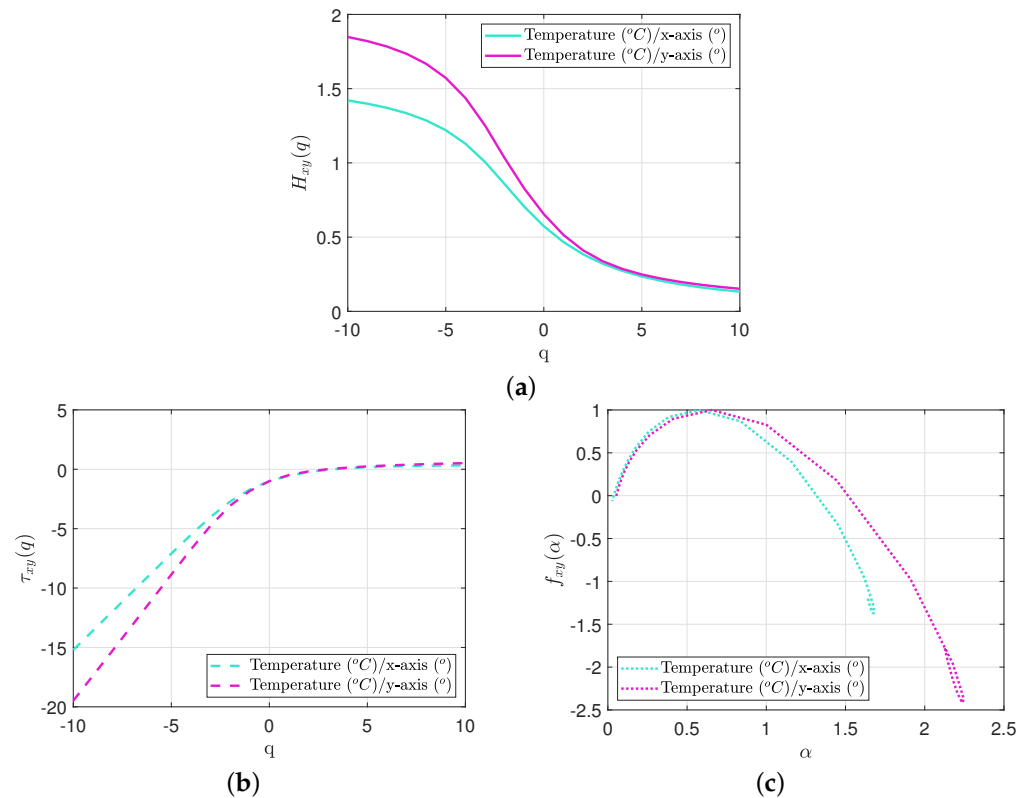


Figure 7. Cross-correlations of (a) the generalized Hurst exponent, (b) Renyi exponent, and (c) multifractal spectrum of two time-series pairs by MF-DCCA.

5. Conclusions

This study preliminarily confirmed the strong correlation between the tilt-angle and temperature time series of transmission line towers using the Pearson correlation coefficient, supported by linear fitting results. Further application of MD-DFA unveiled multifractal characteristics in all three time series. Small fluctuations exhibited positive persistence, while large fluctuations displayed negative persistence. This suggests increased instability in the tilt-angle time series compared to the temperature data, reinforcing the significance of studying their cross-correlation for enhancing power grid engineering design and safety in cold regions. After confirming that all three time series have multifractal characteristics, we used MF-DCCA to test the multifractal cross-correlation characteristics of “Temperature (°C)/x-axis (°)” and “Temperature (°C)/y-axis (°)”, exhibiting negative persistence. Future research could delve into exploring the impact of low-temperature conditions on tower posture and investigating the cross-correlation between temperature and tilt for enhancing power grid engineering design and safety in cold regions, while this study unveiled multifractal cross-correlation between temperature and tilt angles, certain limitations persist. Future research avenues may consider incorporating additional environmental factors affecting tower structures, such as wind speed and precipitation. Furthermore, exploring more intricate multivariate analysis methods to deepen the understanding of relationships between various factors could enhance insights into the stability of transmission tower structures.

Author Contributions: Conceptualization, M.W. and J.W.; methodology, J.W.; software, M.W.; validation, H.G., Z.W., K.Y., C.Z. and G.Z.; formal analysis, G.Z.; investigation, C.Z.; resources, K.Y.; data curation, K.Y.; writing-original draft preparation, M.W.; writing-review and editing, J.W.; supervision, J.W.; project administration, J.W. All authors have read and agreed to the published version of the manuscript.

Funding: The corresponding author Jian Wang expresses thanks to the Natural Science Foundation of Jiangsu Province for support (Grant No BK20240689).

Data Availability Statement: Data are contained within the article.

Conflicts of Interest: Authors Zhigang Wang and Keyu Yue were employed by the company State Grid Jilin Province Electric Power Co., Ltd., Liaoyuan Power Supply Company. The remaining authors declare that the research was conducted in the absence of any commercial or financial relationships that could be construed as a potential conflict of interest.

References

1. Jin, Y.; Wang, W.; Pei, L.; Chen, X.; Song, B. The research and implementation transmission line tower rod and monitoring system using reverse network RTK technology. *J. Phys. Conf Ser.* **2021**, *1894*, 012044. [\[CrossRef\]](#)
2. Guo, J.; Wu, Q.; Guo, K.; Xiong, S.; Feng, W.; Xue, J. Study on the construction and application of digital twins on high voltage transmission line live working scenes. *IEEE Access* **2021**, *9*, 111587–111594. [\[CrossRef\]](#)
3. Abd-Elaal, E.S.; Mills, J.E.; Ma, X. A review of transmission line systems under downburst wind loads. *J. Wind. Eng. Ind. Aerodyn.* **2018**, *179*, 503–513. [\[CrossRef\]](#)
4. Veleđar, M.; Avđaković, S.; Bajramović, Z.; Savić, M.; Stanković, K.; Carsimamović, A. Wavelet-based Analysis of Impulse Grounding Resistance—Experimental Study of the “A”-type Grounding System. *Electr. Power Components Syst.* **2015**, *43*, 2189–2195. [\[CrossRef\]](#)
5. Khodr, H.M. Optimal methodology for the grounding systems design in transmission line using mixed-integer linear programming. *Electr. Power Components Syst.* **2009**, *38*, 115–136. [\[CrossRef\]](#)
6. Wang, C.; Liang, X.; Adajar, E.P.; Loewen, P. Investigation of seasonal variations of tower footing impedance in transmission line grounding systems. *IEEE Trans. Ind. Appl.* **2021**, *57*, 2274–2284. [\[CrossRef\]](#)
7. Gao, J.; Wang, L.; Li, G.; Fang, Y.; Song, B.; Xiao, B.; Liu, K. Discharge of air gaps during ground potential live-line work on transmission lines. *Electr. Power Syst. Res.* **2020**, *187*, 106519. [\[CrossRef\]](#)
8. Xie, Y.L.; Yu, Q.H.; You, Y.H.; Zhang, Z.; Gou, T. The changing process and trend of ground temperature around tower foundations of Qinghai-Tibet Power Transmission line. *Sci. Cold Arid. Reg.* **2019**, *11*, 13–20.
9. Rezaei, S.N.; Chouinard, L.; Langlois, S.; Légeron, F. Analysis of the effect of climate change on the reliability of overhead transmission lines. *Sustain. Cities Soc.* **2016**, *27*, 137–144. [\[CrossRef\]](#)
10. Zhou, W.X. Multifractal detrended cross-correlation analysis for two nonstationary signals. *Phys. Rev. E* **2008**, *77*, 066211. [\[CrossRef\]](#)
11. Kantelhardt, J.W.; Zschiegner, S.A.; Koscielny-Bunde, E.; Havlin, S.; Bunde, A.; Stanley, H.E. Multifractal detrended fluctuation analysis of nonstationary time series. *Physica A* **2002**, *316*, 87–114. [\[CrossRef\]](#)
12. Podobnik, B.; Stanley, H.E. Detrended cross-correlation analysis: A new method for analyzing two nonstationary time series. *Phys. Rev. Lett.* **2008**, *100*, 084102. [\[CrossRef\]](#) [\[PubMed\]](#)
13. Wang, J.; Shao, W.; Kim, J. Analysis of the impact of COVID-19 on the correlations between crude oil and agricultural futures. *Chaos Solitons Fractals* **2020**, *136*, 109896. [\[CrossRef\]](#) [\[PubMed\]](#)
14. Wang, R.; Xie, Y.; Chen, H.; Jia, G. Analyzing the impact of COVID-19 on the cross-correlations between financial search engine data and movie box office. *Fluct. Noise Lett.* **2021**, *20*, 2150021. [\[CrossRef\]](#)
15. Fernandes, L.H.S.; Silva, J.W.L.; de Araujo, F.H.A. Multifractal risk measures by macroeconophysics perspective: The case of brazilian inflation dynamics. *Chaos Solitons Fractals* **2022**, *158*, 112052. [\[CrossRef\]](#)
16. Tsvetkov, V.P.; Mikheev, S.A.; Tsvetkov, I.V.; Derbov, V.L.; Gusev, A.A.; Vinitsky, S.I. Modeling the multifractal dynamics of COVID-19 pandemic. *Chaos Solitons Fractals* **2022**, *161*, 112301. [\[CrossRef\]](#)
17. Wang, J.; Jiang, W.; Yan, Y.; Chen, W.; Kim, J. ECG classification using multifractal detrended moving average cross-correlation analysis. *Int. J. Mod. Phys. B* **2021**, *35*, 2150327. [\[CrossRef\]](#)
18. Xiong, G.; Xiong, Z.; Jia, L.; Truong, T.K. Spatial multifractal spectrum distribution method for breast ultrasonic image classification. *Chaos Solitons Fractals* **2023**, *172*, 113530. [\[CrossRef\]](#)
19. Zhang, R.; Jia, C.; Wang, J. Text emotion classification system based on multifractal methods. *Chaos Solitons Fractals* **2022**, *156*, 111867. [\[CrossRef\]](#)
20. Yin, Y.; Shang, P. Multiscale multifractal detrended cross-correlation analysis of traffic flow. *Nonlinear Dyn.* **2015**, *81*, 1329–1347. [\[CrossRef\]](#)
21. Wang, J.; Shao, W.; Kim, J. Cross-correlations between bacterial foodborne diseases and meteorological factors based on MF-DCCA: A case in South Korea. *Fractals* **2020**, *28*, 2050046. [\[CrossRef\]](#)
22. Zhang, C.; Ni, Z.; Ni, L. Multifractal detrended cross-correlation analysis between PM_{2.5} and meteorological factors. *Physica A* **2015**, *438*, 114–123. [\[CrossRef\]](#)
23. Yu, J.; Sui, L.; Xu, Y.; Chi, B. Fluctuation Characteristics of Water Level and Water Temperature of Huize Well Based on MF-DCCA. *Int. J. Heat Technol.* **2021**, *39*, 825. [\[CrossRef\]](#)
24. Li, G.; Zhang, J.; Wen, X. Electric Power Consumption and Pollutant Emission: A Study Based on DCCA and MF-DCCA. In Proceedings of the 2022 4th Asia Energy and Electrical Engineering Symposium (AEEES), Chengdu, China, 25–28 March 2022; pp. 266–271.

25. Rizvi, S.A.R.; Dewandaru, G.; Bacha, O.I.; Masih, M. An analysis of stock market efficiency: Developed vs. Islamic stock markets using MF-DFA. *Physica A* **2014**, *407*, 86–99. [[CrossRef](#)]
26. Yang, M.; Zhang, Y.; Wang, J. Sign Retention in Classical MF-DFA. *Fractal Fract* **2022**, *6*, 365. [[CrossRef](#)]
27. Wang, J.; Huang, M.; Wu, X.; Kim, J. A local fitting based multifractal detrend fluctuation analysis method. *Physica A* **2023**, *611*, 128476. [[CrossRef](#)]
28. Zunino, L.; Tabak, B.M.; Figliola, A.; Pérez, D.G.; Garavaglia, M.; Rosso, O.A. A multifractal approach for stock market inefficiency. *Physica A* **2008**, *387*, 6558–6566. [[CrossRef](#)]
29. Wen, Z.; Yu, Q.; Zhang, M.; Xue, K.; Chen, L.; Li, D. Stress and deformation characteristics of transmission tower foundations in permafrost regions along the Qinghai–Tibet Power Transmission Line. *Cold Reg. Sci. Technol.* **2016**, *121*, 214–225. [[CrossRef](#)]
30. Harmel, R.D.; Richardson, C.W.; Hanson, C.L.; Johnson, G.L. Evaluating the adequacy of simulating maximum and minimum daily air temperature with the normal distribution. *J. Appl. Meteorol. Climatol.* **2002**, *41*, 744–753. [[CrossRef](#)]
31. Podobnik, B.; Grosse, I.; Horvatić, D.; Ilic, S.; Ivanov, P.C.; Stanley, H.E. Quantifying cross-correlations using local and global detrending approaches. *Eur. Phys. J. B* **2009**, *71*, 243–250. [[CrossRef](#)]
32. Miloš, L.R.; Hațiegan, C.; Miloš, M.C. Multifractal detrended fluctuation analysis (MF-DFA) of stock market indexes. Empirical evidence from seven central and eastern European markets. *Sustainability* **2020**, *12*, 535. [[CrossRef](#)]
33. Mensi, W.; Tiwari, A.K.; Yoon, S.M. Global financial crisis and weak-form efficiency of Islamic sectoral stock markets: An MF-DFA analysis. *Phys. A Stat. Mech. Its Appl.* **2017**, *471*, 135–146. [[CrossRef](#)]

Disclaimer/Publisher’s Note: The statements, opinions and data contained in all publications are solely those of the individual author(s) and contributor(s) and not of MDPI and/or the editor(s). MDPI and/or the editor(s) disclaim responsibility for any injury to people or property resulting from any ideas, methods, instructions or products referred to in the content.